Tracking of dynamic functional connectivity from MEG data with Kalman filtering

Filip Tronarp, Narayan Puthanmadam Subramaniyam, Simo Särkkä and Lauri Parkkonen

Abstract—**Owing to their millisecond-scale temporal resolution, magnetoencephalography (MEG) and electroencephalography (EEG) are well-suited tools to study dynamic functional connectivity between regions in the human brain. However, current techniques to estimate functional connectivity from MEG/EEG are based on a two-step approach; first, the MEG/EEG inverse problem is solved to estimate the source activity, and second, connectivity is estimated between the sources. In this work, we propose a method for simultaneous estimation of source activities and their dynamic functional connectivity using a Kalman filter. Based on simulations, our approach can reliably estimate source activities and resolve their time-varying interactions even at low SNR (<1). When applied on empirical MEG responses to simple visual stimuli, our approach could capture the dynamic patterns of the underlying functional connectivity changes between the lower (pericalcarine) and higher (fusiform and parahippocampal) visual areas. In conclusion, we demonstrate that our approach is capable of tracking changes in functional connectivity at the millisecond resolution of MEG/EEG and thus making it suitable for real-time tracking of functional connectivity, which none of the current techniques are capable of.**

I. Introduction

The two fundamental principles of brain organization are functional segregation and integration that span multiple spatio–temporal scales. Functional integration is usually considered to manifest as functional connectivity, which is defined as statistical interdependencies between brain areas [1] that share functional properties. Recently, the concept of dynamic functional connectivity has become increasingly popular. Using functional magnetic resonance imaging (fMRI), researchers have observed temporal fluctuations in functional connectivity during both rest and execution of specific cognitive tasks [2], [3].

Although several studies have established the dynamic nature of fMRI-derived functional connectivity, fMRI is still an indirect measure of neural activity. In contrast, magnetoencephalography (MEG) and electroencephalography (EEG) are direct measures of electric neural activity and have excellent temporal resolution in the scale of milliseconds. They are thus well-suited for studying dynamic functional connectivity and several studies have already shown that functional connectivity changes over short time intervals [4], [5].

F Tronarp and S Särkkä are with the Department of Electrical Engineering and Automation, and NP Subramaniyam and L Parkkonen are with Department of Neuroscience and Biomedical Engineering, Aalto University, 02150 Espoo, Finland (email:narayan.subramaniyam@aalto.fi). This work was supported by Academy of Finland grant no. 289108 and Aalto ELEC Doctoral School.

However, due to the limited spatial resolution of MEG and EEG, estimating functional connectivity from these signals is not a straightforward task and it typically employs a two-step approach. In the first step, the inverse problem for estimating the source activities in the cortex from MEG or EEG signals is solved, e.g., by using minimum-norm estimation (MNE) [6]. In the second step, anatomical atlases are employed to parcel the cortex to regions of interest (ROI) and the estimated source activities within the ROIs are collapsed to obtain a representative activity time course for each ROI (for example, using flipped mean). Functional connectivity can then be estimated between a subset or all the ROIs using a variety of methods such as phase-locking value (PLV), phase-lag index (PLI), or multivariate autoregressive (MVAR) models, to name a few. A major weakness of the two-step approach is that the estimation of source activity is not informed by the connectivity structure and that connectivity estimation is not informed about the limitations of source estimation (e.g. spatial leakage). Most of the source estimation algorithms used in the Step 1 of the two-step approach assume independence across the sources or ROIs. To introduce additional information during source estimation, linear MVAR models with spatially local interactions and self-interactions were proposed [7], [8]. However, these approaches ignore long-range interactions across brain regions. Furthermore, estimation of dynamic connectivity with two-step approaches that use MVAR models are limited to sliding window analysis and are not capable of estimating connectivity at every time point.

In this work, we propose a novel statistical framework for the simultaneous estimation of source activity and pointwise dynamic connectivity from MEG data. Our approach is based on joint Kalman filtering and uses a state-space model that enables tracking time-varying connectivity. The novelty of our algorithm with respect to other existing one-step approaches [9], [10] is that our approach explicitly allows for statistical dependence between the source activity and their dynamic connectivity, and is suitable for real-time tracking of dynamic functional connectivity.

II. Methodology

A. State-space model

The raw MEG data are assumed to be generated by the following model

$$\mathbf{y}_n = \mathbf{G}\mathbf{q}_n + \mathbf{v}_n$$

where $\mathbf{G}$ is a cortically constrained lead-field matrix, $\mathbf{q}_n$ are the dipole source amplitudes, $\mathbf{v}_n$ is a Gaussian white noise sequence with covariance $\mathbf{R}$, and n is the time index. As we shall consider the tracking a subset of the source amplitudes associated to the anatomical ROIs together with their connectivity, we use the flipped-mean and whitened lead-field given by

$$\mathbf{y}_n = \mathbf{WGH}\mathbf{x}_n + \mathbf{Wv}_n = \mathbf{G}'\mathbf{x}_n + \mathbf{Wv}_n,$$

where $\mathbf{H}$ is the flipped-mean averaging matrix, $\mathbf{W}$ is the whitening matrix, that is $\mathbf{Wv}_n \sim \mathcal{N}(0, \mathbf{I})$. Furthermore, to keep the computational cost down and thus making real-time operation feasible, we shall consider only a subset of the ROIs, write $\mathbf{x}_n^\top = [(\mathbf{x}_n^{(s)})^\top, (\mathbf{x}_n^{(c)})^\top]$ and $\mathbf{G}' = [\mathbf{G}^{(s)}, \mathbf{G}^{(c)}]$, with $\mathbf{x}_n^{(s)}$ denoting source amplitudes to be estimated and $\mathbf{x}_n^{(c)}$ are considered clutter sources[1]. Further assuming $\mathbf{x}_n^{(c)}$ is a white noise sequence with covariance $s\lambda_s \mathbf{I}$ for $s, \lambda_s > 0$, gives the measurement relation

$$\mathbf{y}_n = \mathbf{G}^{(s)}\mathbf{x}_n^{(s)} + \mathbf{e}_n, \tag{1}$$

where $\mathbf{e}_n$ is a white noise sequence with covariance $\mathbf{\Delta} = \mathbf{I} + s\lambda_s \mathbf{G}^{(c)}(\mathbf{G}^{(c)})^\top$. Thus, the measurement error accounts for biological noise. We shall return to appropriate selection of s and λ_s later. Now, in order to track the source amplitude and the connectivity, the following state-space model is used

$$\mathbf{a}_{n+1} = \mathbf{a}_n + \varepsilon_{n+1}^{\mathbf{a}} \tag{2a}$$

$$\mathbf{x}_{n+1} = \mathbf{A}_{n+1}\mathbf{x}_n + \varepsilon_{n+1}^{\mathbf{x}}, \tag{2b}$$

where $\mathbf{x}_n := \mathbf{x}_n^{(s)} \in \mathbb{R}^P$, $\mathbf{a}_n := \operatorname{vec} \mathbf{A}_n \in \mathbb{R}^{P^2}$, $\varepsilon_{n+1}^{\mathbf{a}} \sim \mathcal{N}(0, \mathbf{Q}^{\mathbf{a}})$, and $\varepsilon_{n+1}^{\mathbf{x}} \sim \mathcal{N}(0, \mathbf{Q}^{\mathbf{x}})$. The whole system is then measured according to

$$\mathbf{y}_n = \mathbf{C}\begin{bmatrix} \mathbf{a}_n^\top & \mathbf{x}_n^\top \end{bmatrix}^\top + \mathbf{e}_n, \tag{3}$$

where $\mathbf{C} = \begin{bmatrix} 0 & \mathbf{G}^{(s)} \end{bmatrix}$, with the zero entry corresponds to a zero matrix of an appropriate size.

B. Kalman Filtering

In order to infer the joint state $(\mathbf{a}_n, \mathbf{x}_n)$, a Kalman filter is employed [11]. That is, $(\mathbf{a}_n, \mathbf{x}_n)$ is assumed to be jointly Gaussian distributed,

$$\begin{bmatrix} \mathbf{a}_n \\ \mathbf{x}_n \end{bmatrix} \sim \mathcal{N}\left(\begin{bmatrix} \hat{\mathbf{a}}_n \\ \hat{\mathbf{x}}_n \end{bmatrix}, \begin{bmatrix} \mathbf{\Sigma}_n^{\mathbf{aa}} & \mathbf{\Sigma}_n^{\mathbf{ax}} \\ (\mathbf{\Sigma}_n^{\mathbf{ax}})^\top & \mathbf{\Sigma}_n^{\mathbf{xx}} \end{bmatrix} \right). \tag{4}$$

For short, we write $\mathbf{z}_n^\top = [\mathbf{a}_n^\top, \mathbf{x}_n^\top]$ and $\mathbf{z}_n \sim \mathcal{N}(\hat{\mathbf{z}}_n, \mathbf{\Sigma}_n)$. In order to find a Gaussian approximation to the prediction distribution, the moments $\hat{\mathbf{x}}_{n+1}^-$, $\hat{\mathbf{a}}_{n+1}^-$, $(\mathbf{\Sigma}_{n+1}^{\mathbf{aa}})^-$, $(\mathbf{\Sigma}_{n+1}^{\mathbf{xx}})^-$, and $(\mathbf{\Sigma}_{n+1}^{\mathbf{ax}})^-$ need to computed. This computation can be done in a closed form, using e.g. Isserlis' theorem [12],

$$\hat{\mathbf{x}}_{n+1}^- = \hat{\mathbf{A}}_n \hat{\mathbf{x}}_n + \sum_j (\mathbf{\Sigma}_n^{\mathbf{a}^j\mathbf{x}})_j, \quad \hat{\mathbf{a}}_{n+1}^- = \hat{\mathbf{a}}_n,$$

[1]Suitable re-ordering of $\mathbf{x}_n$ and the columns of $\mathbf{G}'$ is employed

where $(\mathbf{\Sigma}_n^{\mathbf{a}^j\mathbf{x}})_j$ denotes the j:th column of $\mathbb{C}[\mathbf{a}_n^j, \mathbf{x}_n]$ and $\mathbf{a}_n^j$ is the subvector of $\mathbf{a}_n$ corresponding to the j:th column of $\mathbf{A}_n$. Furthermore, the superscript $^-$ denotes a one-step predictive moment. The predicted covariances are given by

$$(\mathbf{\Sigma}_{n+1}^{\mathbf{ax}})^- = \sum_i ((\mathbf{\Sigma}_n^{\mathbf{aa}})_i + \mathbf{Q}_i^{\mathbf{a}})(\hat{\mathbf{x}}_n)_i + (\mathbf{\Sigma}_n^{\mathbf{xa}})^\top \hat{\mathbf{A}}_n^\top$$

$$(\mathbf{\Sigma}_{n+1}^{\mathbf{xx}})^- = \hat{\mathbf{A}}_n \mathbf{\Sigma}_n^{\mathbf{xx}} \hat{\mathbf{A}}_n^\top + \hat{\mathbf{A}}_n \sum_i (\mathbf{\Sigma}_n^{\mathbf{a}_i\mathbf{x}})^\top (\hat{\mathbf{x}}_n)_i$$

$$+ \left(\hat{\mathbf{A}}_n \sum_i (\mathbf{\Sigma}_n^{\mathbf{a}_i\mathbf{x}})^\top (\hat{\mathbf{x}}_n)_i \right)^\top + \sum_{i,j} \mathbf{\Sigma}_n^{\mathbf{a}_i\mathbf{x}} \mathbf{e}_j \mathbf{e}_i^\top (\mathbf{\Sigma}_n^{\mathbf{a}_j\mathbf{x}})^\top$$

$$+ \sum_{i,j} (\mathbf{Q}_{ij}^{\mathbf{a}} + \mathbf{\Sigma}_n^{\mathbf{a}_i\mathbf{a}_j})((\mathbf{\Sigma}_n^{\mathbf{xx}})_{ij} + (\hat{\mathbf{x}}_n)_i (\hat{\mathbf{x}}_n)_j) + \mathbf{Q}^{\mathbf{x}}$$

$$(\mathbf{\Sigma}_{n+1}^{\mathbf{aa}})^- = \mathbf{\Sigma}_n^{\mathbf{aa}} + \mathbf{Q}^{\mathbf{a}}$$

where $\mathbf{Q}_i^{\mathbf{a}}$ and $(\mathbf{\Sigma}_n^{\mathbf{aa}})_i$ are the i:th block columns of $\mathbf{Q}^{\mathbf{a}}$ and $\mathbf{\Sigma}_n^{\mathbf{aa}}$ of size $P^2 \times P$, respectively. Furthermore, $\mathbf{Q}_{ij}^{\mathbf{a}}$ denotes the $P \times P$ block in $\mathbf{Q}^{\mathbf{a}}$ at position (i, j), $(\mathbf{\Sigma}_n^{\mathbf{xx}})_{ij}$ is the element of $\mathbf{\Sigma}_n^{\mathbf{xx}}$ at position (i, j), $(\hat{\mathbf{x}}_n)_i$ is the i:th element of $\hat{\mathbf{x}}_n$, $\mathbf{e}_i$ is a canonical basis vector of appropriate dimension, lastly $\mathbf{\Sigma}_n^{\mathbf{a}_i\mathbf{a}_j}$ is the cross-covariance matrix between the i:th and the j:th columns of $\mathbf{A}_n$. The predictive mean and covariances can then be collected into $\hat{\mathbf{z}}_{n+1}^-$ and $\mathbf{\Sigma}_{n+1}^-$ for which the filter mean of $\mathbf{z}_{n+1}$ can be obtained by the Kalman update [11]

$$\mathbf{S}_{n+1} = \mathbf{C}\mathbf{\Sigma}_{n+1}^- \mathbf{C}^\top + \mathbf{\Delta} \tag{7a}$$

$$\mathbf{K}_{n+1} = \mathbf{\Sigma}_{n+1}^- (\mathbf{G}^{(s)})^\top \tag{7b}$$

$$\hat{\mathbf{z}}_{n+1} = \hat{\mathbf{z}}_{n+1}^- + \mathbf{K}_{n+1}(\mathbf{y}_{n+1} - \mathbf{C}\hat{\mathbf{z}}_{n+1}^-) \tag{7c}$$

$$\mathbf{\Sigma}_{n+1} = \mathbf{\Sigma}_{n+1}^- - \mathbf{K}_{n+1}\mathbf{S}_{n+1}\mathbf{K}_{n+1}^\top. \tag{7d}$$

C. Heuristics For Parameter Setup

It is important to select the parameters, $\mathbf{Q}^{\mathbf{a}}, \mathbf{Q}^{\mathbf{x}}, s$, and λ_s appropriately to achieve adequate tracking performance. The covariance matrix $\mathbf{Q}^{\mathbf{a}}$ determines the trade-off between tracking performance and smoothness of the connectivity parameter trajectories; in our experiments $\mathbf{Q}^{\mathbf{a}} = \mathbf{I}/10$ to $\mathbf{Q}^{\mathbf{a}} = \mathbf{I}/1000$ appears adequate. The selection of the rest of the parameters is inspired by the heuristics for choosing the regularization parameter in standard MNE. Firstly, we set $\mathbf{Q}^{\mathbf{x}} = \lambda_s \mathbf{I}$ and then assume that the contribution to the measurements of each clutter source in $\mathbf{x}_n^{(c)}$ is a couple of orders of magnitude less than those in $\mathbf{x}_n$, which means s is small; in our experiments we use $s = 1/100$. Lastly, assuming $\mathbf{x}_n$ and $\mathbf{x}_n^{(c)}$ are white-noise sequences, the relation between the signal-to-noise ratio (SNR) and λ_s is given by

$$\lambda_s = \frac{(\mathrm{SNR})^2 p_y}{\operatorname{tr}\{\mathbf{G}^{(s)}(\mathbf{G}^{(s)})^\top\} + s\operatorname{tr}\{\mathbf{G}^{(c)}(\mathbf{G}^{(c)})^\top\}}. \tag{8}$$
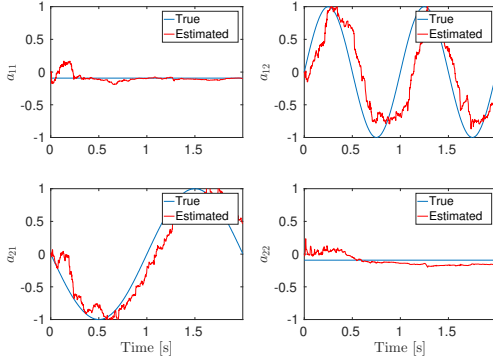
where p_y is the number of MEG sensors.

Fig. 1. Exemplary plot of true and estimated AR coefficients for SNR = 0.1

Fig. 2. Real MEG data. Estimated source activities in the three ROIs averaged across trials. The shaded regions represents 95% CI.

III. SIMULATIONS AND REAL MEG DATA

A. Simulation setup

We simulated dynamic connectivity between two sources (see Figure 1) using the following time-varying MVAR model

$$x_{1,n+1} = a_{11,t}x_{1,n} + a_{12,t}x_{2,n} + \epsilon^x_{1,n+1}$$
$$x_{2,n+1} = a_{21,t}x_{1,n} + a_{22,t}x_{2,n} + \epsilon^x_{2,n+1}$$

where $a_{11,t}$ and $a_{22,t} \sim \mathcal{N}(\mu, \sigma_1)$. The cross-interaction terms are given as $a_{12,t} = \sin(2 * \pi * t) + v(t)$ and $a_{21,t} = \sin(2*\pi*0.5*t) + v(t)$, where $v(t) \sim \mathcal{N}(0, \sigma_2)$. MEG data were simulated at varying signal-to-noise ratios (SNR) using a three-compartment realistically-shaped boundary element model (BEM) for the head, provided by the MNE-software [13], that included the surfaces of inner skull, outer skull and skin with conductivities 0.3 S/m, 0.06 S/m and 0.3 S/m, respectively. The source space was created using octahedron subdivision and fixed source orientation normal to the local cortical surface, resulting in approximately 8000 source dipoles distributed evenly across the cortical mantle.

B. MEG data

To facilitate comparison of methods, we used the publicly-available "MNE sample" dataset [13] that comprises recordings with the 306-channel whole-scalp neuromagnetometer. For the purpose of this study, we used only the responses to visual stimuli (checkerboard patterns presented to the left visual field). The preprocessed data consisted of 67 trials of 700 ms (–200 ms before and 500 ms after stimulus onset) duration. The head model used was again from the MNE sample data (see Section III-A). Based on the anatomical Desikan–Killiany atlas, we predefined the following ROIs, roughly corresponding to lower and higher visual areas in the right hemisphere: 1) pericalcarine-rh, 2) fusiform-rh and 3) parahippocampal-rh.

IV. RESULTS AND DISCUSSION

Figure 1 shows an exemplary plot of the true and estimated AR coefficients for one Monte-Carlo run at SNR = 0.1. Even at low SNR, our approach is able to track the time-varying AR coefficients that reflect the self-interaction of and
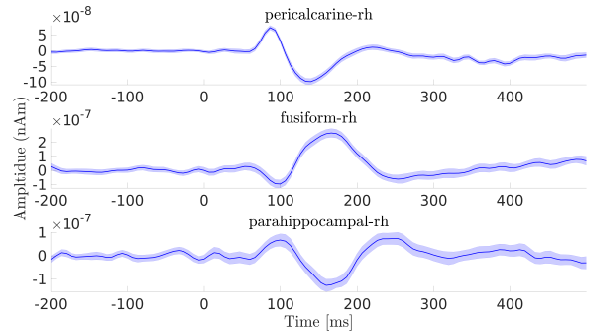
TABLE I
SIMULATION RESULTS. THE MEAN RMSE COMPUTED ACROSS TIME AND 100 MONTE-CARLO SIMULATIONS FOR VARYING SNR.

States	SNR = 0.1	0.5	1	3	5
x_1	0.63	0.36	0.27	0.17	0.13
x_2	0.63	0.37	0.28	0.17	0.13
a_{11}	0.05	0.03	0.02	0.02	0.02
a_{12}	0.39	0.29	0.26	0.25	0.25
a_{21}	0.28	0.19	0.17	0.16	0.16
a_{22}	0.05	0.02	0.02	0.02	0.02

the cross-interaction between the sources. We quantify the reconstruction errors in Table I, where we show the results from 100 Monte-Carlo realizations for varying SNR. The mean RMSE values shown in the table are computed across all the time points and across the 100 Monte-Carlo runs.

For the real MEG responses, source activations and dynamic functional connectivity averaged over all the trials are shown in Figures 2 and 3, along with 95% confidence intervals (CI). From Fig. 2 it can be seen that the source activity in pericalcarine-rh and fusiform-rh ROIs shows positive peaks at around 100 ms and 150 ms, respectively, after the stimulus onset. These peaks are related to the first major visually-evoked responses originating in the primary visual cortex (the striate cortex within the calcarine fissure) and higher-order cortices in the fusiform gyrus [14].

Figures 3 and 4 demonstrate that the functional connectivities estimated between the three ROIs clearly show different patterns over time. In particular, we see that the pericalcarine-rh region has a feedforward influence on fusiform-rh and parahippocampal-rh region, as reflected by the shift in the functional connectivity dynamics after the stimulus onset (first row of Fig. 3). However, no significant shifts in the connectivity were found for the reverse direction, i.e., from fusiform-rh or parahippocampal-rh to pericalcarine-rh (first column of Fig. 3). These preliminary results are intriguing as they indicate that our method is able to recover transient changes in functional connectivity between lower and higher level visual areas. We also performed a two-tailed t-test to compare the mean of the baseline of functional connectivity (–200 to 0 ms) to functional connectivity at each time point.
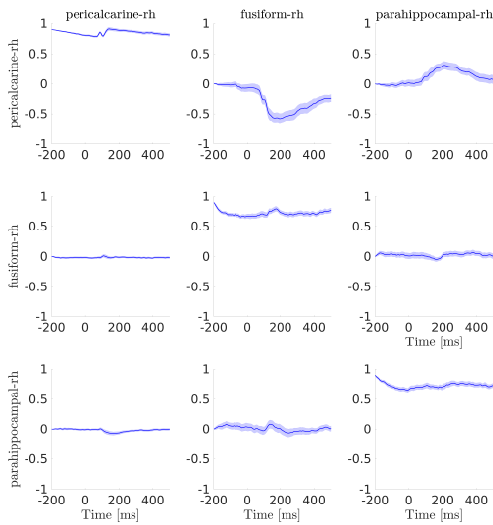
Fig. 3. Time-varying interactions between the three ROIs. The first row represents self-interaction for pericalcarine-rh and feedforward interaction from pericalcarine-rh to fusiform-rh and parahippocampal-rh. Middle and bottom rows are to be interpreted similarly.
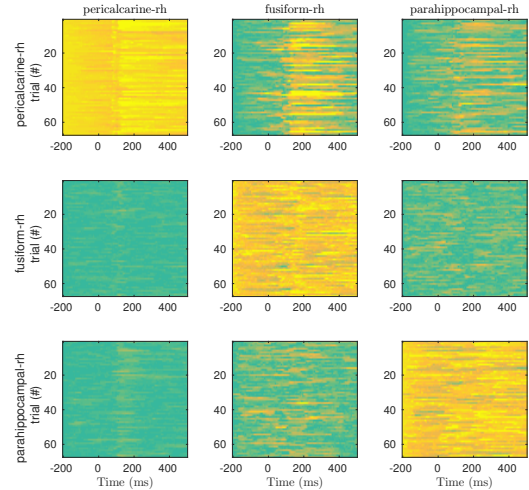

Fig. 4. Time–Epoch plot of the connectivity parameters. The epoch (trial) number is on the vertical axis and time on the horizontal axis. The color scale is fixed to $[-1, 1]$, and brighter colors correspond to larger $|A_{ij}|$.

Our results revealed significant changes in connectivity ($p < 0.05$, Bonferroni-corrected) in the direction pericalcarine-rh $\rightarrow$ fusiform-rh and pericalcarine-rh $\rightarrow$ parahippocampal-rh.

This functional connectivity is likely due to evoked activity, i.e. due to the evoked responses elicited in the visual cortices studied. Focusing on time periods void of evoked responses or subtracting them from the data before estimating connectivity may reveal functional connectivity driven by ongoing activity.

We make a short note on computational complexity. Since the Kalman filter scales cubically with the state dimension, our method has computational complexity $O(P^6)$. Nevertheless, in our experiments even $P = 5$ appears feasible for real-time operation, though the method can be scaled for more ROIs with an optimized software implementation.

V. CONCLUSIONS

We have demonstrated that our functional connectivity estimation approach based on joint Kalman filtering can reliably estimate source activity and track changes in functional connectivity even at low SNRs. When applied to real MEG data, our approach could describe the temporal dynamics in functional connectivity between lower- and higher-order visual areas. In the future, we will apply our method to complex visual stimuli, hypothesized to elicit both feedforward and feedback connections across visual areas.

REFERENCES

[1] K. J. Friston, "Functional and Effective Connectivity: A Review," *Brain Connectivity*, vol. 1, no. 1, pp. 13–36, Jan. 2011.
[2] E. Simony, C. J. Honey, J. Chen, O. Lositsky, Y. Yeshurun, A. Wiesel, and U. Hasson, "Dynamic reconfiguration of the default mode network during narrative comprehension," *Nature Communications*, vol. 7, p. 12141, Jul. 2016.
[3] A. Kucyi, M. J. Hove, M. Esterman, R. M. Hutchison, and E. M. Valera, "Dynamic Brain Network Correlates of Spontaneous Fluctuations in Attention," *Cerebral Cortex (New York, N.Y.: 1991)*, vol. 27, no. 3, pp. 1831–1840, Mar. 2017.
[4] M. J. Brookes, G. C. O'Neill, E. L. Hall, M. W. Woolrich, A. Baker, S. Palazzo Corner, S. E. Robson, P. G. Morris, and G. R. Barnes, "Measuring temporal, spectral and spatial changes in electrophysiological brain network connectivity," *NeuroImage*, vol. 91, pp. 282–299, May 2014.
[5] G. C. O'Neill, M. Bauer, M. W. Woolrich, P. G. Morris, G. R. Barnes, and M. J. Brookes, "Dynamic recruitment of resting state subnetworks," *NeuroImage*, vol. 115, pp. 85–95, Jul. 2015.
[6] M. S. Hämäläinen and R. J. Ilmoniemi, "Interpreting magnetic fields of the brain: minimum norm estimates," *Medical & Biological Engineering & Computing*, vol. 32, no. 1, pp. 35–42, Jan. 1994.
[7] A. Galka, O. Yamashita, T. Ozaki, R. Biscay, and P. Valdés-Sosa, "A solution to the dynamical inverse problem of EEG generation using spatiotemporal Kalman filtering," *NeuroImage*, vol. 23, no. 2, pp. 435–453, Oct. 2004.
[8] M. Fukushima, O. Yamashita, A. Kanemura, S. Ishii, M. Kawato, and M.-a. Sato, "A state-space modeling approach for localization of focal current sources from MEG," *IEEE transactions on bio-medical engineering*, vol. 59, no. 6, pp. 1561–1571, Jun. 2012.
[9] M. Fukushima, O. Yamashita, T. R. Knösche, and M.-a. Sato, "MEG source reconstruction based on identification of directed source interactions on whole-brain anatomical networks," *NeuroImage*, vol. 105, pp. 408–427, Jan. 2015.
[10] N. P. Subramaniyam, F. Tronarp, S. Särkkä, and L. Parkkonen, "Expectation–maximization algorithm with a nonlinear Kalman smoother for MEG/EEG connectivity estimation," in *EMBEC & NBC 2017*, ser. IFMBE Proceedings. Springer, Singapore, Jun. 2017, pp. 763–766, dOI: 10.1007/978-981-10-5122-7_191.
[11] S. Särkkä, *Bayesian filtering and smoothing*. Cambridge University Press, 2013, vol. 3.
[12] L. Isserlis, "On a formula for the product-moment coefficient of any order of a normal frequency distribution in any number of variables," *Biometrika*, vol. 12, no. 1/2, pp. 134–139, 1918.
[13] A. Gramfort, M. Luessi, E. Larson, D. A. Engemann, D. Strohmeier, C. Brodbeck, R. Goj, M. Jas, T. Brooks, L. Parkkonen, and M. Hämäläinen, "MEG and EEG data analysis with MNE-Python," *Frontiers in Neuroscience*, vol. 7, 2013.
[14] F. Di Russo, A. Martínez, M. I. Sereno, S. Pitzalis, and S. A. Hillyard, "Cortical sources of the early components of the visual evoked potential," *Human Brain Mapping*, vol. 15, no. 2, pp. 95–111, Feb. 2002.